



## Journal of Advanced Research in Fluid Mechanics and Thermal Sciences

Journal homepage:  
[https://semarakilmu.com.my/journals/index.php/fluid\\_mechanics\\_thermal\\_sciences/index](https://semarakilmu.com.my/journals/index.php/fluid_mechanics_thermal_sciences/index)  
ISSN: 2289-7879



# Comparative Assessment of Turbulence Models for Predicting Square Cyclone Separator Performance

Cut Indah Nurul Izzah<sup>1</sup>, Yunardi<sup>4,\*</sup>, Mutia Reza<sup>2</sup>, Novi Sylvia<sup>3</sup>, Nur Malahayati<sup>4</sup>, Farid Mulana<sup>4</sup>, Michael Fairweather<sup>5</sup>

<sup>1</sup> Chemical Engineering Postgraduate Program, Faculty of Engineering, Universitas Syiah Kuala, Banda Aceh 23111, Indonesia

<sup>2</sup> Department of Chemical Engineering, Kalimantan Institute of Technology, Balikpapan 76127, Indonesia

<sup>3</sup> Department of Chemical Engineering, Faculty of Engineering, Universitas Malikussaleh, Lhokseumawe, North Aceh, Indonesia

<sup>4</sup> Department of Chemical Engineering, Universitas Syiah Kuala, Banda Aceh 23111, Indonesia

<sup>5</sup> School of Chemical and Process Engineering, University of Leeds, Leeds LS2 9JT, United Kingdom

### ARTICLE INFO

#### Article history:

Received 12 September 2024

Received in revised form 29 December 2024

Accepted 10 January 2025

Available online 10 February 2025

#### Keywords:

Square cyclone; simulation; turbulence models; collection efficiency; pressure drop

### ABSTRACT

As with conventional cyclones, the gas-particle flow within a square cyclone is characterized by the consistent presence of turbulence. Therefore, selecting an appropriate turbulence model to accurately predict cyclone performance is crucial. This paper presents the findings of a computational fluid dynamics (CFD) study that assesses the impact of various turbulence models on the flow field, collection efficiency, and pressure drop predictions within square cyclone separators. In the simulation of the flow field, an investigation was conducted into five turbulence models falling under the Reynolds Averaged Navier-Stokes category, namely the Spalart-Allmaras, standard  $k-\epsilon$ , RNG  $k-\epsilon$ , standard  $k-\omega$ , and Reynolds Stress models. Each turbulence model was coupled with a discrete phase model to represent solid particle flow within a square cyclone. The solution of the flow and particle transport equations was conducted using the software Ansys Fluent (version 21.1). Except for the flow field, for which experimental data were unavailable, the calculations were validated by comparing the predicted results for the square cyclone overall and grade efficiencies, and the pressure drop, with values from the literature. The findings of this simulation investigation demonstrate that all tested turbulence models exhibit comparable qualitative trends in predicting the tangential and axial velocity profiles. However, when evaluated in quantitative terms, the RNG  $k-\epsilon$  model tends to overpredict both the tangential and axial velocities compared to the other models. Conversely, in the majority of cases, the  $k-\epsilon$  standard turbulence model tends to underpredict these velocities in comparison to the other models. Regarding the predictions of the square cyclone performance, the Reynolds Stress Model is particularly noteworthy among the five turbulence models examined. It provides qualitative and quantitative closer agreement with the experimental data regarding the overall collection, grade efficiencies, and pressure drop. In general, while all models produced qualitatively similar trends in square cyclone performance predictions, the Reynolds Stress Model yielded the closest agreement with the experimental results, both qualitatively and quantitatively.

\* Corresponding author.

E-mail address: [yunardi@usk.ac.id](mailto:yunardi@usk.ac.id)

<https://doi.org/10.37934/arfmts.127.1.140160>

## 1. Introduction

Cyclones are ubiquitous in industrial processes, providing a simple yet effective means of separating particulate matter from gas streams. Technological advances, initially designed for dust collection, have led to the use of cyclones in dryers and reactors. However, particle collection remains the most common application and plays a key role in meeting stringent air quality standards. The high collection efficiency, simple design, cost-effectiveness, and low maintenance requirements of cyclones offer distinct advantages over other air pollution-control systems. Cyclones are capable of operating under a wide range of conditions, including high temperature and pressure. Cyclones are typically used as pre-cleaning units prior to more sophisticated controls, such as electrostatic precipitators, scrubbers, or baghouses. Additionally, cyclones are often used as final collectors, particularly for large particles [1]. Their versatility, reliability, and longevity will ensure that cyclones remain an integral part of industrial gas cleaning in the foreseeable future. With ongoing research improving cyclone designs to increase collection efficiency, these simple yet robust units will continue to serve as important air pollution control technologies.

A cyclone consists of four main components that have a decisive influence on its separation efficiency: the inlet, cylinder body, vortex finder, and outlet. The operating principle is simple and involves the tangential introduction of a gas-solid mixture via the upper cyclone inlet. This imparts a spinning motion to the particles inside the cylindrical section, causing them to move towards the walls by the action of the centrifugal force. The gas stream then spiralled downwards until it reached the conical section. At this point, the rotational velocity is sufficient to prevent further particle-wall collisions. At the base of the cone, the gas reverses its direction and flows upward into the vortex finder duct before exiting the cyclone. The separated particles settled in the hopper for subsequent collection. Meanwhile, the cleaned gas rotated upwards out of the vortex finder. This complex flow pattern and geometry ensured an efficient separation. The efficiency of a cyclone depends on several factors, including the operating parameters and dimensions of the inlet, cylinder, cone, and vortex finder [2]. Ongoing research is aimed at optimizing these design factors and operating conditions to improve cyclone separation performance for both current and emerging applications.

For almost two centuries, cyclone bodies had a conventional cylindrical shape with a design that originated in the 19th century. This long-standing tradition broke in the early 1990s with the introduction of the square cyclone, which was a radical departure from the convention [3,4]. The square cyclone concept was developed based on the specific requirements of circulating fluidized bed (CFB) technology, which has become a prominent low-emission coal combustion system. CFB boilers are commercially available and highly regarded for their efficiency and environmental benefits. The separator plays a key role in CFB performance and has a direct influence on reliability and design. In the context of coal combustion, the primary function of the separator is to remove materials, such as unburned coal and ash, from the flue gas and return them to the furnace to extend the residence time and enable desulfurization. Although conventional cyclones have historically performed this function, limitations have become apparent in the context of large CFB boilers. The need for substantially thick refractory walls in the construction of large cylindrical cyclones results in significant delays at the start of the operating cycle. This issue was addressed in 1991 with the introduction of the Ahlstrom Pyroflow Compact CFB boiler, which uses a square cyclone separator [5]. Despite a reduction in collection efficiency, square cyclones offer several advantages, including compactness, shorter start-up time, simpler structure, and lower cost [6]. These advantages make square cyclones an attractive option for large CFB boilers, where efficiency, reliability, and cost-effectiveness are paramount. The use of square cyclones has been extended to new applications by redesigning the traditional cyclone shapes.

The basic principles of the separation techniques used in square cyclones are similar to those used in their conventional counterparts. Both types rely on the generation of centrifugal force by swirling airflow to achieve gas-solid particle separation [7]. In a square cyclone, the gas flow enters through an inlet and undergoes a series of changes in direction as it traverses a rectangular chamber. This complex trajectory results in turbulent flow patterns and the generation of a centrifugal force field within the chamber. As a result of these dynamic forces, the particles were forced to separate from the gas stream and descend to the lower part of the chamber. To improve the efficiency of this particle separation process and to optimize the design dimensions of the cyclone separator, it is essential to gain an in-depth understanding of the turbulent flow dynamics and behaviour of solid particles within the separator. This knowledge is critical for fine-tuning the design and operating parameters of square cyclones to ensure efficient and reliable gas-solid particle separation in a range of industrial applications.

Since their introduction, several experimental studies have been carried out to gain insight into the turbulent flow and particle dynamics behaviour within square cyclones. These studies have been instrumental in advancing our understanding of the performance of square cyclones. Su and Mao [8] used a three-dimensional particle dynamics analyser (3D-PDA) to measure the flow of gas and solid particles in a square cyclone separator with a downward gas outlet. Several cases were investigated by varying the inlet velocity and the particle concentration. Glass beads with an average diameter of 30-40  $\mu\text{m}$  were used for the tests. The results of the study showed that the flow field deviated from the centre of the cyclone with a Rankine vortex pattern and local vortices at the corners. Quasi-laminar particle motion increased turbulence at the corners owing to collisions, resulting in a higher turbulent kinetic energy. The pressure drop occurred mainly at the corners, which facilitated particle separation by dissipating the kinetic energy. This study provides valuable insights into the complex dynamics of gas-solid flows in cyclone separators. One of the techniques used in the study by Wasilewski *et al.*, [9] was Particle Image Velocimetry (PIV), which was developed in the late 1970s. PIV is an invaluable tool for improving the velocity measurements in fluid dynamics experiments. This technique allows velocity distribution data to be recorded simultaneously at multiple spatial points, providing a detailed view of fluid flow characteristics under specific conditions. It is important to note that despite the widespread use of PIV for the measurement of cyclonic flows, the data obtained by this method are still insufficient to fully capture the intricacies of flow behaviour [10]. The limitations of this technique include constraints related to time, cost, and the inherent complexity of gas-particle dynamics within square cyclones. Taken together, these factors make it almost impossible to obtain a comprehensive representation of the entire flow field phenomenon through fluid dynamic experiments alone. However, advances in computational fluid dynamics (CFD) and high-speed computing have opened new avenues for research. The advent of advanced computational techniques has enabled researchers to model and analyse complex flow phenomena within square cyclones. These include the intricate aspects of turbulence, multi-phase flow, and fluid-structure interactions. As a result, numerous simulation studies have been conducted to explore the complex flow-field dynamics within square cyclones. These simulations provide valuable insights that complement the experimental data and contribute to a more comprehensive understanding of square cyclone performance.

In a simulation study, Raoufi *et al.*, [11] investigated and evaluated flow dynamics within a square cyclone separator. Researchers used the Reynolds Stress Model (RSM) to create a computational model of the gas flow patterns within the separator. The simulation results provide interesting insights into the tangential velocity profiles at different sections of the square cyclone. The profiles revealed the existence of a swirling flow pattern consisting of two distinct components: an outer free vortex and an inner forced vortex located at the centre. These results are similar to those observed

in conventional cyclones. Another notable study by Su *et al.*, [12] used RSM to simulate the dynamics of gas flow in square cyclone separators. In addition, a Lagrangian approach was used to represent the particle dynamics within the square separators. This study investigated the effect of different gas discharge configurations on the performance of square cyclones. The results showed that changing the gas outlet from a circular to a square configuration of the equivalent cross-section resulted in an increase in the collection efficiency while reducing the pressure drop.

The use of RSM has attracted considerable interest among researchers modelling the flow field within square cyclones [13-15]. It is important to acknowledge that although the RSM provides comprehensive insights, it requires more computational time than the RNG k-ε model, which is commonly used to simulate conventional cyclones [16]. Despite the RSM being the predominant turbulence model used to simulate flow dynamics within square cyclones, there is a paucity of studies investigating alternative turbulence models for this purpose. This is in contrast to the approach taken with conventional cyclones, where a variety of turbulence models have been used to investigate the flow dynamics and their effect on separator performance. This study presents the results of performance evaluations carried out on five Reynolds-averaged Navier-Stokes (RANS) turbulence models: Spalart-Allmaras, standard k-ε, RNG k-ε, k-ω, and RSM. The main objective of this study was to evaluate the performance of five Reynolds Averaged Navier-Stokes turbulence models in predicting the flow field within a square cyclone separator and their subsequent impact on the pressure drop and efficiency. The predictions generated by each model were rigorously validated by comparison with available experimental data [8]. This thorough analysis improves our understanding of the dynamics involved in square cyclone separators, leading to improved optimization of their performance for various industrial applications.

## 2. Methodology

### 2.1 Turbulence and Particle Dynamics Modelling

A comprehensive three-dimensional computational fluid dynamics (CFD) simulation was performed to elucidate the complex flow patterns within the square cyclone separator. In this simulation, the turbulent gas entering the square cyclone was considered to be an incompressible isothermal Newtonian fluid in a steady state. The governing equations that encapsulate the fluid flow behaviour within the separator include the continuity equation and Reynolds-averaged Navier-Stokes equations, which can be succinctly expressed as Eq. (1) and Eq. (2).

$$\frac{\partial \bar{u}_i}{\partial x_i} = 0 \quad (1)$$

$$\bar{u}_i \frac{\partial \bar{u}_i}{\partial x_j} = -\frac{1}{\rho} \frac{\partial \bar{p}}{\partial x_i} + \nu \frac{\partial^2 \bar{u}_i}{\partial x_j \partial x_j} - \frac{\partial}{\partial x_i} (\overline{u'_i u'_j}) \quad (2)$$

where  $\bar{u}_i$  is the mean velocity,  $x_i$  is the position,  $\bar{p}$  is the mean pressure,  $\rho$  is the constant air density,  $\nu$  is the kinematic viscosity, and  $\overline{u'_i u'_j}$  is the Reynolds stress tensor. To account for the Reynolds stresses introduced by the averaging process, they must be modelled in terms of the averaged flow parameters to complete the set of governing equations. In turbulent viscosity-based models, the closure of Reynolds stresses is achieved by establishing a relationship between the turbulent viscosity and mean velocity gradients.

$$\frac{\partial}{\partial t} (\rho \tilde{\nu}) \frac{\partial}{\partial x_i} (\rho \tilde{\nu} u_i) = C_{b1} \rho \tilde{S} \tilde{\nu} + \frac{1}{\sigma_p} \left[ \frac{\partial}{\partial x_j} \left( (\mu + \rho \tilde{\nu}) \frac{\partial \tilde{\nu}}{\partial x_j} \right) + C_{b2} \rho \left( \frac{\partial \tilde{\nu}}{\partial x_j} \right)^2 \right] - \rho f_w \left( \frac{\tilde{\nu}}{d} \right)^2 + S_v \quad (3)$$

The Spalart-Allmaras turbulence model, shown in Eq. (3), is a one-equation approach that relies on a single transport equation for eddy viscosity to account for the turbulence effects. Unlike two-equation models, such as the  $k-\epsilon$  and  $k-\omega$  models, the Spalart-Allmaras model does not explicitly solve for Reynolds stresses. Alternatively, the Reynolds stresses are considered indirectly by including a production term in the transport equation for turbulent viscosity. The model uses the turbulent kinetic energy and its dissipation rate, both of which are related to Reynolds stresses, to calculate the production term. This production term reflects the rate at which the mean velocity gradient generates turbulent kinetic energy and is directly proportional to Reynolds stress. For more detailed information on the definitions and values of the relevant constants and additional equations relevant to the Spalart-Allmaras model, Meza and Medina [17] can be consulted.

The standard  $k-\epsilon$  turbulence model provides a more comprehensive approach than the previous single-equation models. The model establishes a fundamental link between Reynolds stresses in turbulent flows and turbulent kinetic energy and relates the dissipation of this energy to the dissipation rate. In particular, the model uses two different equations: one governing the turbulent kinetic energy ( $k$ ), which quantifies the energy from turbulent fluctuations, and another governing the dissipation rate ( $\epsilon$ ), which quantifies the conversion of turbulent kinetic energy into thermal energy by molecular viscosity. The transport equations for turbulent kinetic energy and its dissipation are given in Eq. (4) and Eq. (5), respectively: The model is widely recognized for its application in various industrial scenarios; however, it may have limitations when dealing with complex flow conditions, such as those involving unfavourable pressure gradients.

$$\frac{\partial}{\partial t}(\rho k) + \frac{\partial}{\partial x_i}(\rho k u_i) = \frac{\partial}{\partial x_j} \left[ \left( \mu + \frac{\mu_t}{\sigma_k} \right) \frac{\partial k}{\partial x_j} \right] - G_k + G_b - \rho \epsilon - Y_M + S_k \quad (4)$$

$$\frac{\partial}{\partial t}(\rho \epsilon) + \frac{\partial}{\partial x_i}(\rho \epsilon u_i) = \frac{\partial}{\partial x_j} \left( \alpha_\epsilon \mu_{eff} \frac{\partial \epsilon}{\partial x_j} \right) + C_{1\epsilon} \frac{\epsilon}{k} (G_k + C_{1\epsilon} G_b) - C_{2\epsilon} \rho \frac{\epsilon^2}{k} + S_\epsilon \quad (5)$$

The  $k-\epsilon$  turbulence model offers several advantages that contribute to its popularity as a means of simulating turbulent flows in the context of CFD. In particular, the model is widely used in CFD simulation due to its ease of implementation and computational efficiency. While it effectively models many turbulent flows, it has limitations in accurately capturing complex flows with significant streamline curvature or separation. Despite these shortcomings, the  $k-\epsilon$  model has proven successful in simulating flow fields within conventional cyclones [17].

The RNG  $k-\epsilon$  turbulence model used in this study was an extension of the standard  $k-\epsilon$  model. It was designed to alleviate some of the limitations of the latter in predicting turbulence in complex flows. Similar to the standard  $k-\epsilon$  model, it uses two transport equations to calculate the turbulence kinetic energy ( $k$ ) and dissipation rate ( $\epsilon$ ). However, the RNG  $k-\epsilon$  model is distinguished by the inclusion of an additional term within the dissipation rate equation, specifically, to account for the influence of the Reynolds number on turbulence. The additional term within the dissipation equation improves the accuracy of the model, particularly in high-Reynolds-number scenarios. High-Reynolds-number flows are prevalent in many practical engineering applications. Consequently, the RNG  $k-\epsilon$  model is considered more reliable than the standard  $k-\epsilon$  model in capturing the complex behaviour of turbulence in these high Reynolds number flows.

The standard  $k-\omega$  turbulence model, which is based on the premise that turbulence within a flow can be effectively characterized by two length scales, the turbulence kinetic energy ( $k$ ) and turbulence dissipation rate ( $\omega$ ), was also used in the current study. This model treats turbulence by solving two transport equations: Eq. (6) for  $k$ , and Eq. (7) for  $\omega$ . These equations quantify the rate of

turbulence generation and dissipation within the flow, providing a detailed representation of the turbulent behaviour present in the system.

$$\frac{\partial}{\partial t}(\rho k) + \frac{\partial}{\partial x_i}(\rho k u_i) = \frac{\partial y}{\partial x_j} \left( \Gamma_k \frac{\partial k}{\partial x_j} \right) + G_k - Y_k + S_k \quad (6)$$

$$\frac{\partial}{\partial t}(\rho \omega) + \frac{\partial}{\partial x_i}(\rho \omega u_i) = \frac{\partial y}{\partial x_j} \left( \Gamma_\omega \frac{\partial \omega}{\partial x_j} \right) + G_\omega - Y_\omega + S_\omega \quad (7)$$

where  $G_k$  and  $G_\omega$  represent the generations of  $k$  and  $\omega$ , respectively;  $\Gamma_k$  and  $\Gamma_\omega$  are the effective diffusivities of  $k$  and  $\omega$ , respectively; and  $Y_k$  and  $Y_\omega$  represent the dissipation of  $k$  and  $\omega$ , respectively.

The RSM, the last turbulence model within the Reynolds-averaged Navier–Stokes (RANS) category considered in this study, represents a more complicated approach than the widely used standard  $k$ – $\varepsilon$  model. The main difference lies in the RSM's ambition to model the full Reynolds stress tensor, rather than focusing solely on the turbulent kinetic energy and its dissipation rate, as illustrated in Eq. (8).

$$\begin{aligned} \frac{\partial}{\partial t} R_{ij} + \bar{u}_k \frac{\partial}{\partial x_k} R_{ij} = \frac{\partial}{\partial x_k} \left( \frac{\nu_t}{\partial^k} \frac{\partial}{\partial x_k} R_{ij} \right) - \left[ R_{ik} \frac{\partial \bar{u}_j}{\partial x_k} + R_{jk} \frac{\partial \bar{u}_k}{\partial x_k} \right] - C_1 \frac{\varepsilon}{K} \left[ R_{ij} - \frac{2}{3} \delta_{ij} K \right] - \\ C_2 \left[ P_{ij} - \frac{2}{3} \delta_{ij} P \right] - \frac{2}{3} \delta_{ij} \varepsilon \end{aligned} \quad (8)$$

where  $P_{ij}$ , the term for the turbulence production is expressed as Eq. (9) [11].

$$P_{ij} = - \left[ R_{ik} \frac{\partial \bar{u}_j}{\partial x_k} + R_{jk} \frac{\partial \bar{u}_k}{\partial x_k} \right], P = \frac{1}{2} P_{ij} \quad (9)$$

The transport equation for turbulence dissipation in the RSM is given by Eq. (10).

$$\frac{\partial \varepsilon}{\partial t} + \partial \bar{u}_j \frac{\partial \varepsilon}{\partial x_j} = \frac{\partial}{\partial x_j} \left( \nu + \frac{\nu_t}{\partial^k} \frac{\partial}{\partial x_j} \right) - C^{\varepsilon 1} \frac{\varepsilon}{K} R_{ij} \frac{\partial \bar{u}_i}{\partial x_j} - C^{\varepsilon 2} \frac{\varepsilon^2}{K} \quad (10)$$

Indeed, the Reynolds Stress model has the potential to provide more accurate results than simpler turbulence models, especially in scenarios involving complex geometries and flows characterized by high levels of turbulence anisotropy. Its ability to capture intricate interactions and the anisotropic nature of turbulence can be particularly advantageous under these challenging conditions. However, it is important to recognize that the increased complexity of the RSM results in certain trade-offs. The process of implementing and verifying the model may become more arduous because of the increased computational requirements.

It is common practice to use both the Eulerian-Eulerian and Eulerian-Lagrangian approaches in the modelling of multiphase flows. In this study, the Eulerian-Lagrangian approach was used to predict the tracking of particles in a two-phase gas-solid flow within a cyclone. In this approach, the gas phase (air) is treated as a continuous medium, whereas solid particles are treated as discrete entities dispersed within this gas phase. A discrete phase model (DPM) technique was used to predict particle tracking within the cyclone and to calculate the collection efficiency. This technique assumes that the interactions between solid particles are negligible because of their low concentrations. Consequently, it uses a one-way coupling approach that focuses on the effect of the fluid flow field on the motion of the individual particles. Consequently, the equations governing the particle dynamics within the cyclone can be formulated as shown in Eq. (11) and Eq. (12) [18]. These

equations offer a means to characterize and predict the behaviour of solid particles within the gas-solid flow, facilitating the assessment of the collection efficiency in the cyclone.

$$\frac{du_{pi}}{dt} = \frac{18\mu}{\rho_p d_p^2} \frac{C_D Re_p}{24} (u_i - u_{pi}) + \frac{g_i(\rho_p - \rho)}{\rho_p} \quad (11)$$

$$\frac{dx_{pi}}{dt} = u_{pi} \quad (12)$$

where  $u_i$  and  $u_{pi}$  are the gas and particle velocities in the  $i$  direction, respectively.  $\rho_p$  and  $\rho$  represent the particle and air densities, respectively, and  $\mu$  is the gas dynamic viscosity.  $C_D$  and  $Re_p$  represent the drag coefficient and relative Reynolds number, respectively, and  $d_p$  and  $g_i$  denote the particle diameter and gravitational acceleration in the  $i$  direction, respectively.

## 2.2 Flow Configuration and Numerical Simulation

The geometric parameters and schematic representation of the square cyclone used in the simulation study are shown in Figure 1(a). In addition, Table 1 lists the values of the various parameters of the cyclones used in both the experimental and numerical investigations. Notably, all the data presented in Table 1 are consistent with the experimental conditions documented in the study by Su and Mao [8], which serves as the basis for validating the results of the current study, ensuring their accuracy and reliability. A structured hexahedral mesh was used to effectively discretize the entire computational domain by dividing the domain into 300,697 individual cell grids. Figure 1(b) shows the layout of this mesh, highlighting the grid structure used in the numerical simulations. In this study a uniform mesh was selected to achieve its convergence within a cyclone simulation, thereby ensuring that the results remain unaffected by variations in mesh elements. The test indicated stable convergence across all turbulence models, suggesting that the selected mesh effectively captures flow phenomena. The implementation of a uniform mesh is advantageous as it minimizes the risk of significant numerical diffusion, particularly in transitional or wake regions. Furthermore, it facilitates a more reliable assessment of computational complexity, especially for simpler geometries such as square cyclones. This methodology not only reduces the preparation time for simulations but also consistently produces dependable results in studies concerning mesh independence. Within the context of a square cyclone, the primary flow structure is predominantly located in the main volume, allowing a uniform mesh to adequately capture detailed flow patterns in proximity to the walls. Previous studies have demonstrated that the use of a uniform mesh in square cyclones results in convergent outcomes without disproportionately concentrating the mesh in wall areas [14].

A three-dimensional computational fluid dynamics (CFD) simulation was used to represent the flow field inside the square cyclone separator. The turbulent gas entering the square cyclone can be treated as an incompressible dilute two-phase gas-solid turbulent flow. The simulation represents the gas phase as air, characterized by uniform parameters, such as a density of  $1.225 \text{ kg/m}^3$  and a viscosity of  $1.7894 \times 10^{-5} \text{ kg/m.s}$ . In the solid phase, the particles were introduced into the square cyclone via the inlet surface. The particles are introduced into the cyclone with an initial velocity of zero and a concentration of  $8.8 \text{ g/m}^3$  at the inlet. The density of the individual particles was measured to be  $1989.7 \text{ kg/m}^3$ , and their diameters ranged from 8 to  $30 \text{ }\mu\text{m}$ .

The numerical solution to the previously described equations was obtained using the ANSYS Fluent (v21.1) commercial CFD software. The control volume method was used to discretize the transport equations. This technique provides a viable strategy for converting the governing

equations, which are continuous, into a discrete form that can be easily solved using computational methods. The PISO approach was used for the numerical solution, which is essential for the accurate and efficient resolution of the pressure-velocity coupling. This algorithm is considered the optimal choice for the current computation. The use of the Quadratic Upwind Interpolation for Convective Kinematics (QUICK) method facilitated the accurate representation of flow dynamics, ensuring the maintenance of numerical stability and the accurate representation of sharp variations in flow variables. The PRESTO technique was used to evaluate the pressure interpolation process in numerical solution methods, ensuring accurate computation of pressure fields to obtain reliable data from CFD simulations.

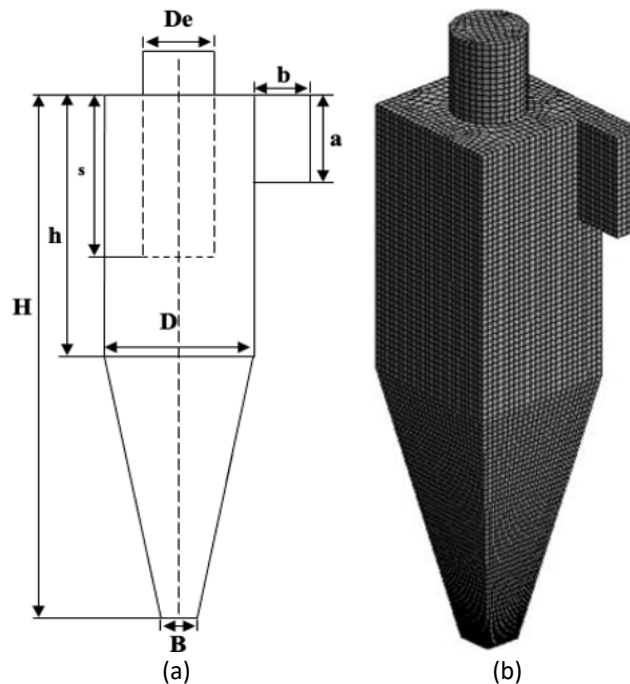


**Fig. 1.** Schematic diagram of (a) the square cyclone and (b) its generated mesh

**Table 1**

Geometrical dimensions of the square cyclone used in the simulation

Parameter	Symbol	Value (mm)
Cyclone body diameter	D	200
Inlet height	a	150
Inlet width	b	40
Inlet thickness	a'	75
Vortex finder diameter	De	100
Length of vortex finder	S	240
Cyclone body length	h	400
Cyclone length	H	800
Duct diameter	B	50

### 3. Results and Discussion

#### 3.1 The Flow Field Inside the Square Cyclone

The velocity distribution within a conventional or square cyclone can be described by three velocity components: tangential, axial, and radial. The term 'tangential velocity' is used to describe the speed at which a fluid rotates or swirls as it undergoes circular or spiral motion within a cyclone.

The generation of centrifugal force is a critical element in the cyclone separation process because it facilitates the separation of particles. The term "axial velocity" is used to describe the linear motion of the fluid along the axis of the cyclone. This refers to the velocity of the fluid in the axial direction, whether it enters the cyclone or exits through the vortex finder. The radial velocity refers to the velocity component either towards or away from the centre of the cyclone. This phenomenon has the potential to influence the trajectory of particles, guiding them towards the inner walls of the cyclone to facilitate their separation. However, the radial velocity is often considered less important than the tangential and axial velocities, resulting in frequent omissions in fundamental calculations [19].

As with conventional models, the tangential velocity is considered the most important factor influencing the performance of a square cyclone separator. The principle of separation in a cyclone is based on the generation of centrifugal forces as a result of the vortex motion. The centrifugal force allows denser particles or droplets to move towards the periphery of the cyclone, while lighter gases or particles tend to remain near the centre and exit through the vortex finder. The efficiency of the particle separation in a cyclone is closely related to the magnitude and consistency of the tangential velocity profile [20]. It follows that the analysis and prediction of the flow field, in this case, the tangential velocity within the square cyclone, is of both theoretical and practical importance in improving the efficiency of the cyclone separator.

Figure 2 shows a comparison of the tangential velocity predictions generated by different turbulence models, namely the RSM, Spalart-Allmaras,  $k-\epsilon$  standard,  $k-\epsilon$  (re-normalization group RNG), and standard  $k-\omega$  models, with respect to their radial positions within the square cyclone. The velocity was predicted at an axial position 400 mm ( $y=2D$ ) from the bottom of the square cyclone. All turbulence models show a consistent qualitative trend, namely that the tangential velocity profile has two peaks on either side of the off-centre line of the cyclone, with the lowest peak occurring exactly at the centre line. The predicted profiles provide compelling evidence for the existence of two distinct components within the cyclone chamber vortex flow: an outer free vortex and an inner solid rotation near the centre. The RNG  $k-\epsilon$  turbulence model produces peak tangential velocity values in the outer midpoint region that exceed those predicted by the RSM model. However, it gives predictions in the inner vortex region that are comparable to those predicted by the RSM. In contrast, the standard  $k-\epsilon$  turbulence model consistently predicts the lowest tangential velocity in the outer and inner vortex regions. The differences in predictions between the standard  $k-\epsilon$  and RNG  $k-\epsilon$  turbulence models are due to key methodological advances in the RNG variant. Unlike the conventional  $k-\epsilon$  model, the RNG model incorporates a more sophisticated epsilon dissipation rate equation and explicitly accounts for the effects of swirling and rotation on turbulent flow dynamics. These refinements enable the RNG  $k-\epsilon$  model to more accurately capture complex flow characteristics, particularly in scenarios involving intricate vortex structures where the standard  $k-\epsilon$  model exhibits reduced predictive capabilities.

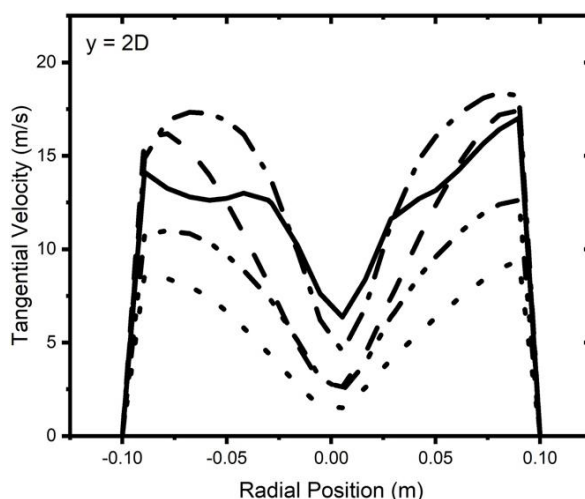


**Fig. 2.** Comparison between tangential velocity predictions by various turbulence models (prediction results; - RSM; - - Spalart-Allmaras; .... k- $\epsilon$  standard; - · - RNG k- $\epsilon$ ; - · · - k- $\omega$  standard)

In the absence of direct experimental data to validate flow field predictions, selecting the most appropriate turbulent model for a square cyclone is a challenging task. Nevertheless, the Reynolds Stress Model (RSM) has shown the most promising results among the available modelling approaches. Fatahian and Fatahian [21] used the RSM model to investigate the flow characteristics within a square cyclone. Although they lacked experimental data specific to the flow field, they validated their model against experimental measurements of collection efficiency and pressure drop, which showed remarkably close agreement with the collected data [8]. Consequently, the RSM model was adopted to predict the flow field in the square cyclone, providing a qualitative representation that is consistent with the objectives of the present study. This superiority can be attributed to the ability of the RSM to handle complex flows with rotational flows and vortices, which are common features of cyclones.

The efficiency of particle or material collection in any type of cyclone can be optimized by controlling the axial velocity. It is of paramount importance to ensure that the particles are transported effectively and that they do not escape into the main gas or fluid stream. Furthermore, an adequate axial velocity plays a significant role in the prevention of re-entrainment, which has the potential to reduce the separation efficiency by carrying separated particles back into the gas or fluid stream. The occurrence of re-entrainment can be minimized by maintaining sufficient axial velocity [22].

In addition to tangential velocity, axial velocity is a significant factor in the collection of particles within a cyclone. Figure 3 shows a comparative analysis of the axial velocity within the studied square cyclone using different turbulence models, including the RSM, Spalart-Allmaras, k- $\epsilon$  standard, RNG k- $\epsilon$ , and k- $\omega$ . This y-velocity distribution was measured at the connection position between the conical and cyclone bodies, or 400 mm from the bottom of the square cyclone. The experimental trend indicated that the y-velocity in the near-wall region was downward, with a greater amount on the right side [15]. At the centre of the cyclone, the numerical result demonstrates an upward y-velocity, which is in good agreement with the experimental data in this region. The visualization shows a consistent trend across all turbulence models, with the highest axial velocity observed in the central region of the cyclone and the lowest velocities along the walls and cone section. However, notable discrepancies exist between these models in terms of their quantitative accuracy.

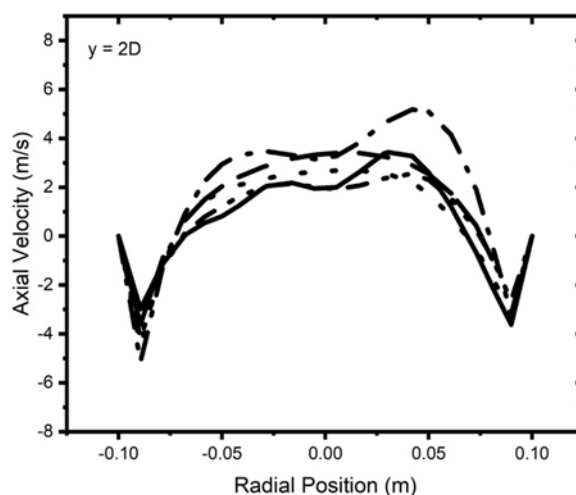
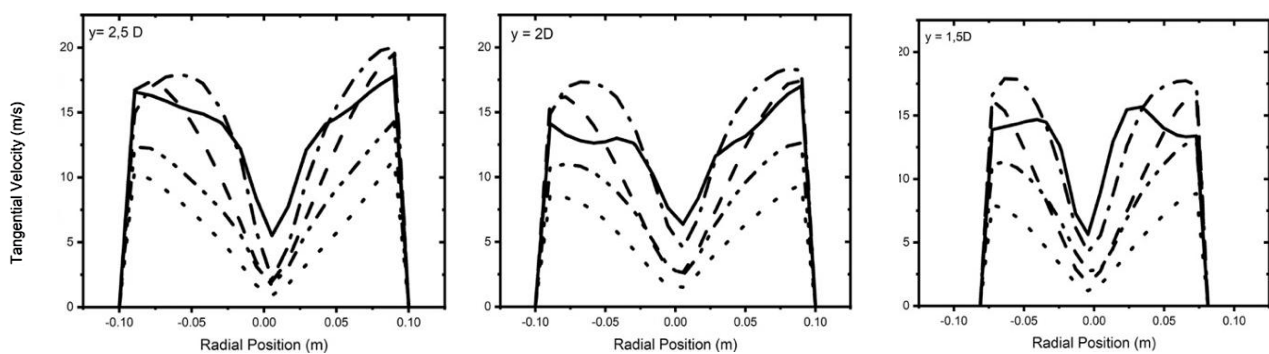


**Fig. 3.** Comparison between predicted axial velocity by various turbulence models (predicted results; — RSM; - - Spalart-Allmaras; .... k- $\epsilon$  standard; - · - RNG k- $\epsilon$ ; - · · - k- $\omega$  standard)

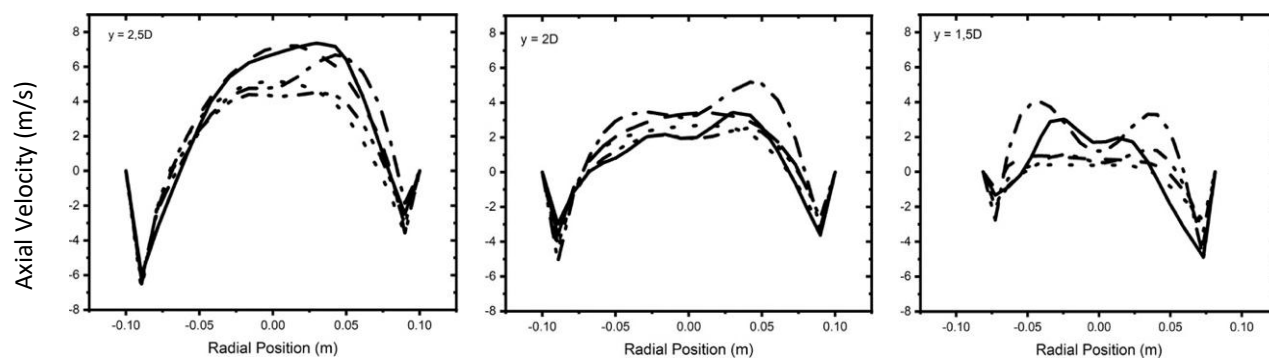
The RNG k- $\epsilon$  turbulence model consistently predicts the highest tangential and axial velocity values, with its qualitative results closely mirroring those of the RSM turbulence model. The RSM offers a distinctive axial velocity profile within the square cyclone, providing a comprehensive representation of the velocity distribution. The visualization indicates that the RSM prediction reveals a moderate velocity magnitude, effectively reflecting the fundamental flow dynamics. Notably, the model successfully captures the experimental observation trend of downward velocity in the near-wall region, particularly on the right side of the cyclone. The RSM predicts an increase in velocity as the flow transitions to the central zone, closely aligning with the experimental data and demonstrating a smooth, progressive velocity gradient. The profile indicates that maximum axial velocities are concentrated in the central region, gradually diminishing toward the walls and cone section. In contrast to previous turbulence models, the RSM employs a balanced approach, avoiding the exaggerated velocity predictions commonly associated with models such as the RNG k- $\epsilon$ , while providing a more nuanced and physically accurate depiction of the flow field within the square cyclone.

Figure 4 and Figure 5 show the velocity distribution of the tangential and axial components at three specific axial locations: 1.5D, 2D, and 2.5D. It is worth noting that designations 2.5D and 2D refer to specific locations on the body of the cyclone, whereas positions 1.5D are located on the conical side of the cyclone. When analyzing Figure 3 and Figure 4, it is clear that a recognizable pattern emerges. Specifically, as the transition is made from the 2.5D position to the 1.5D position, both the tangential and axial velocities exhibit a noticeable decrease. The figures in this analysis indicate that positive velocity values correspond to an upward flow orientation, whereas negative values indicate a downward flow. It is worth noting that the decrease in axial velocity is particularly pronounced in the conical section, reaching a value close to zero or even slightly negative. The variation in axial velocity within a cyclone or conical structure arises from the distribution of fluid flow, which is influenced by the device's geometry, centrifugal force, and pressure dynamics. In a cyclone, the axial velocity increases on the right side due to the interplay between tangential and axial flow. As the fluid rotates, denser particles are propelled toward the outer wall by centrifugal force, while lighter fluid concentrates nearer to the centre. The cyclone generates two principal flow patterns: the outer vortex (descending) and the inner vortex (ascending). In this design, the downward flow (outer vortex) predominates, exhibiting higher axial velocities on the right side due

to asymmetric pressure distribution and the impact of the Coriolis force on turbulent flow, particularly in cyclones with distinct geometric characteristics. The fluid's tangential entry creates flow asymmetry, leading to increased axial velocities to the right, determined by the vortex rotation direction and inlet geometry. The reduced cross-sectional area in the conical portion compels the flow to accelerate. As the internal vortex intensifies around the cyclone's centre, the velocity distribution may shift leftward, especially if there is an interaction between the internal vortex and radial pressure. Within the conical section, the upwardly driven internal vortex increasingly prevails, often resulting in a higher axial velocity distribution to the left, due to its interaction with the conical wall and the pressure pattern intrinsic to the conical section. However, the decrease in tangential velocity is comparatively less significant and shows a consistent pattern over many positions, namely 1.5D, 2D, and 2.5D. This finding suggests that changes in the axial position have a more pronounced effect on the axial velocity than the tangential velocity, which has a fairly stable pattern across the axial positions.



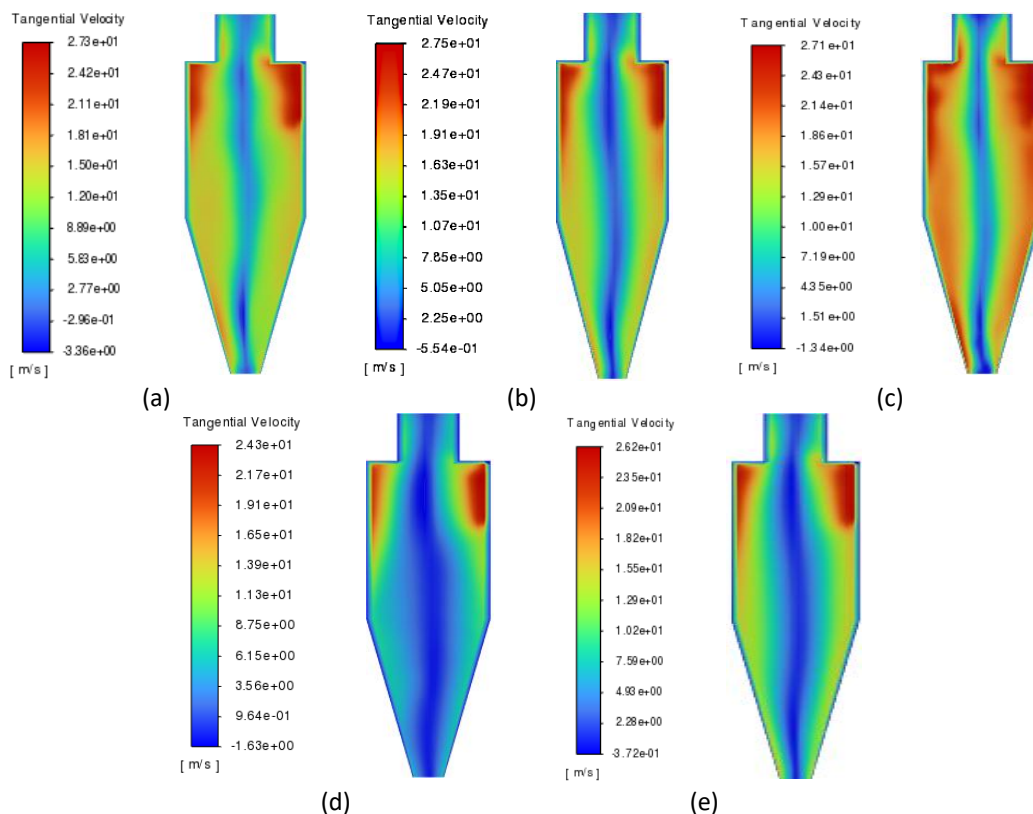
**Fig. 4.** Predicted tangential velocities at three positions  $y = 1.5 D$ ,  $y = 2.0 D$  and  $y = 2.5 D$  (predicted results; – RSM; – – Spalart-Allmaras; ··· k- $\epsilon$  standard; - · - RNG k- $\epsilon$ ; - · - k- $\omega$  standard)



**Fig. 5.** Predicted axial velocity at three positions  $y = 1.5 D$ ,  $y = 2.0 D$  and  $y = 2.5 D$  (predicted results; – RSM; – – Spalart-Allmaras; ··· k- $\epsilon$  standard; - · - RNG k- $\epsilon$ ; - · - k- $\omega$  standard)

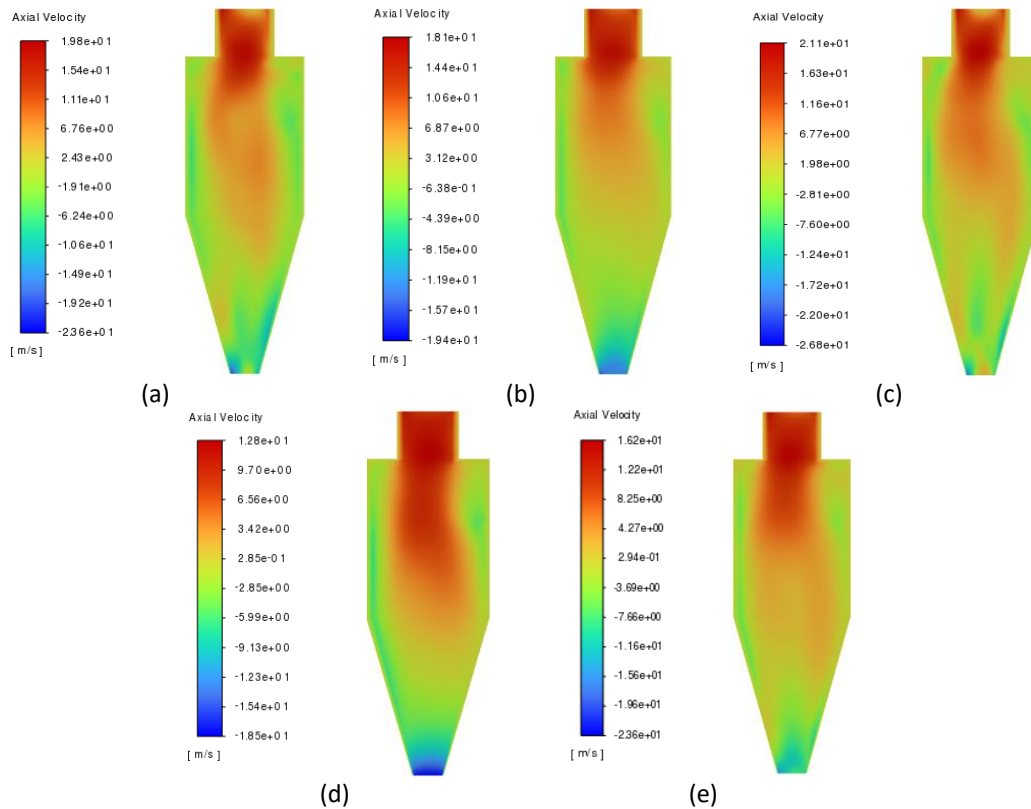
A simulation of the flow field in a circular cyclone conducted by Safikhani *et al.*, [23] revealed tangential velocity profiles that were closely aligned with those observed in this study. The similarity between the tangential velocity curve patterns in square cyclones and conventional cyclones underlines the fundamental principle of fluid dynamics that transcends specific configurations. This principle is relevant to various fluid flow scenarios beyond cyclones. In both square and circular cyclones, the primary forces at play are centrifugal force, pressure gradients, and viscous forces. These forces interact consistently regardless of the shape of the cyclone, resulting in analogous velocity profiles. This similarity illustrates the underlying physics governing fluid behaviour, allowing more effective modelling and optimization across different cyclone designs.

Contours illustrating the tangential and axial velocities for different models, namely, the Reynolds Stress Model (RSM), Spalart-Allmaras, RNG k- $\epsilon$ , k- $\epsilon$  standard, and k- $\omega$ , are presented in Figure 6 and Figure 7. These contours were generated at an inlet velocity of 20.21 m/s. The simulation findings demonstrate that the contour forms of both the tangential and relative axial velocities exhibit consistency among the models, with variations predominantly evident in the maximum and minimum contour values. The tangential velocity contours shown in Figure 6 demonstrate a striking consistency in the upper region of the square cyclone across all turbulence models analyzed. This uniformity in flow patterns highlights a strong agreement among the different turbulent models in predicting the flow dynamics within this important area of the cyclone. The observed similarity is especially significant for cyclone performance, as the upper region is crucial for the initial separation process. These findings closely align with the simulation results reported by Surahmanto *et al.*, [24], which further validate the methods and outcomes of the current study. The highest velocities were concentrated near the edges of the cyclone, as indicated by the red and orange regions. This rapid rotational flow along the walls was crucial for the particle separation mechanism of the cyclone. It generates the centrifugal force required to separate particles based on their mass. On the other hand, the central region of the cyclone exhibits the lowest tangential velocity, as indicated by the dark blue contours. This low-velocity core is characteristic of cyclone separators and contributes to the overall flow dynamics.



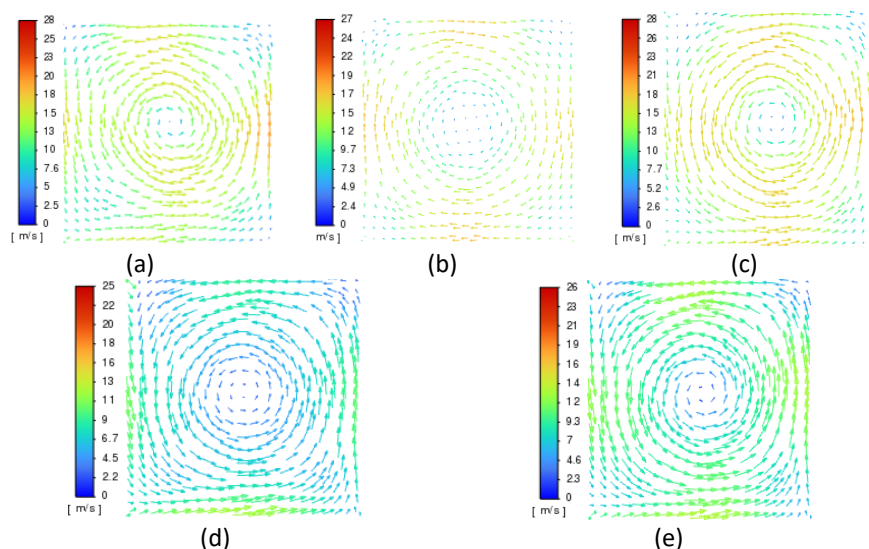
**Fig. 6.** Tangential velocity contours simulated by various turbulence models (a) RSM, (b) Spalart-Allmaras, (c) RNG k- $\epsilon$ , (d) k- $\epsilon$  standard, and (e) k- $\omega$  standard

Figure 7 shows the axial velocity contours, which provide additional information on the vertical component of the flow, thus complementing the tangential velocity data. In all models, there was a consistent presence of positive axial velocities (flowing upward) in the central region of the cyclone, particularly near the vortex finder. This upward flow is critical for transporting lighter particles from the cyclones. In contrast, negative axial velocities (flowing downwards) were observed along the cyclone walls and conical section. This downward flow helps collect heavier particles and directs them to the bottom of the cyclone for separation.



**Fig. 7.** Axial velocity contours computed by various turbulence models (a) RSM, (b) Spalart-Allmaras, (c) RNG  $k-\epsilon$ , (d)  $k-\epsilon$  Standard, and (e)  $k-\omega$

Furthermore, computational simulations were performed to predict the velocity vectors of a square cyclone with a vertical dimension of 400 mm, encompassing both tangential and axial velocities. The velocity vector depicted in Figure 8 reveals the complexities of flow behaviour prediction. The RSM turbulence model yielded the highest and most precise values compared with the prediction simulation data provided by Su *et al.*, [12]. The Spalart-Allmaras model is simpler but may underpredict flow complexity, especially in high shear and rotation regions. The RNG  $k-\epsilon$  model is intermediate between RSM and standard  $k-\epsilon$ , offering a balance between accuracy and computational cost. The standard  $k-\epsilon$  model is more uniform but may oversimplify the flow in high curvature and rotation regions. The  $k-\omega$  model is similar to the  $k-\epsilon$  models, but with distinct differences, showing a better prediction of near-wall flows and more pronounced secondary flows in the corners. The choice of turbulence model has profound implications for square cyclone modelling, with RSM being the most accurate; however, its computational cost is potentially prohibitive for some applications.



**Fig. 8.** Velocity vector provided by various turbulence models (a) RSM, (b) Spalart-Allmaras, (c) RNG k- $\epsilon$ , (d) k- $\epsilon$  Standard, and (e) k- $\omega$

### 3.2 Particle Trajectory

The movement of particles within a cyclone strongly determines the outcome of cyclone separation. The direction and trajectory of the particles are influenced by various critical parameters such as the intrinsic properties of the particles, their initial velocity upon entry, and the concentration or quantity of particles introduced into the cyclone. It is crucial to acknowledge that the selection of a turbulence model for the prediction of particle mobility in a cyclone results in discernible particle behaviour.

Flow simulation in cyclones aims to elucidate the dynamics of particle motion influenced by turbulent flow. Figure 9 shows the particle motion predictions generated by the DPM in combination with various turbulence models under similar entry conditions. These conditions consisted of an entry velocity of 20.21 m/s and a total of 50 particles. The analysis of particle trajectories reveals a distinct and complex distribution of vortices, with particles typically adhering closely to the turbulent flow structure. The core vortex exhibits stability, characterized by a circular arrangement of particles surrounding the cyclone's central region. Additionally, small vortices and complex turbulence features are observable in both the core region and near the cyclone wall.

The Reynolds Stress Model (RSM) provides a comprehensive and accurate prediction of particle trajectories within a cyclone by solving the complete transport equations corresponding to each component of the Reynolds Stress tensor. This methodological capability enables the RSM to effectively capture complex turbulence behaviour, in particular, the turbulence anisotropy often observed in cyclone systems. In such contexts, turbulent flow is significantly influenced by centrifugal forces, drag, and velocity fluctuations, all of which affect particle trajectories. The RSM directly models these interactions, providing a more realistic representation compared to conventional isotropic models such as k- $\epsilon$ . By calculating detailed velocity fluctuations, the RSM accounts for the interplay between turbulent flow and particles, which is critical for accurately modelling small particles that exhibit increased sensitivity to local velocity fluctuations. The Euler-Lagrange approximation used in the RSM improves the accuracy of particle trajectory calculations by skillfully modelling the interaction between particles and the turbulent flow field. In addition, the model effectively captures phenomena such as vortex breakdown and backflow in the central region of the cyclone, which significantly affect particle distribution - effects that are often overlooked or simplified

in less complex turbulence models. For larger particles with significant inertia, the RSM continues to reliably predict velocity gradients and intricate flow patterns. Several simulation studies, including that of Hoekstra *et al.*, [25], show that RSM produces particle distribution predictions that closely match experimental data, especially for cyclones with complex flow distributions. Consequently, RSM is the preferred option for analyses that require high accuracy, especially in contexts with significant turbulence gradients and simulations of inhomogeneous turbulent flows in cyclones; however, it requires considerable computational time due to the complexity of the governing equations.

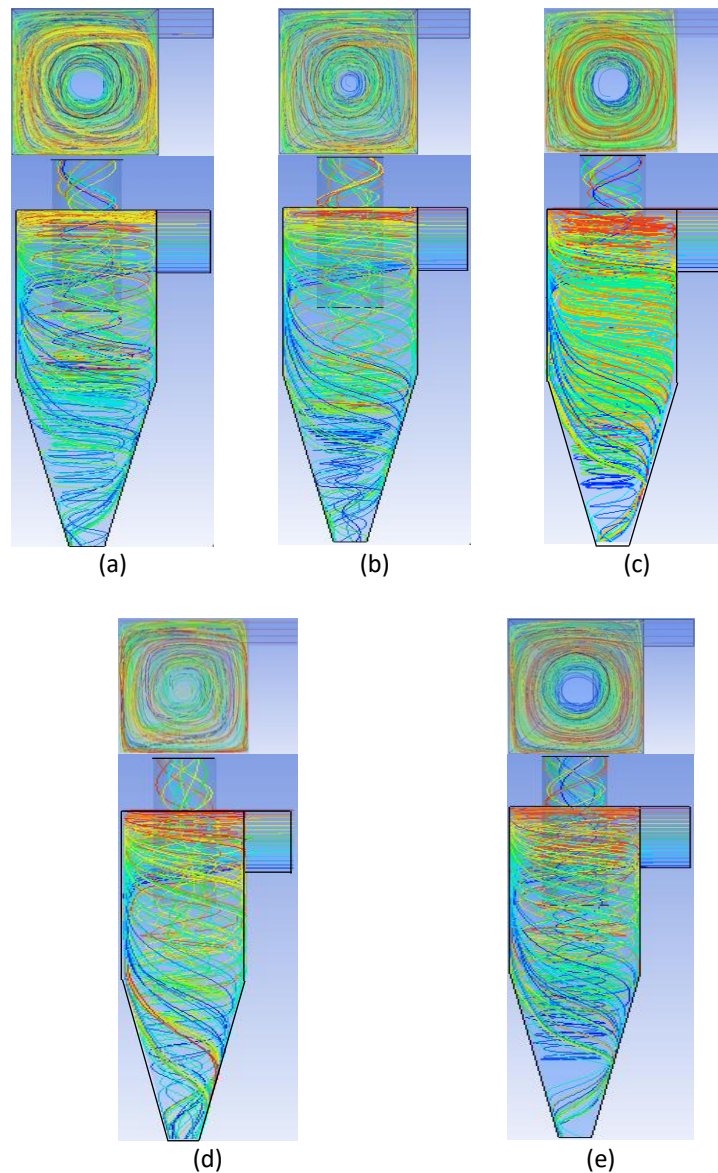


**Fig. 9.** The trajectory of particles in a cyclone by various turbulence models (a) RSM, (b) Spalart-Allmaras, (c) RNG  $k-\epsilon$ , (d)  $k-\epsilon$  Standard, and (e)  $k-\omega$

The comparative analysis of other turbulence models reveals distinct particle trajectory characteristics across different approaches. The Spalart-Allmaras model, being a one-equation model, produces the simplest trajectories with linear particle movements, making it most suitable for initial simulations. The RNG  $k-\epsilon$  model offers enhanced rotational motion and greater trajectory complexity, providing a balance between accuracy and computational efficiency for moderate turbulence scenarios. The standard  $k-\epsilon$  model generates less pronounced vortices with unstable

particle distributions, while the  $k-\omega$  model excels in capturing near-wall flow interactions. Despite their strengths, these models share limitations in fully representing the anisotropic and complex flow structures within cyclones, with the RSM model generally providing the most detailed representation of particle dynamics.

### 3.3 Prediction and Validation of the Efficiency and Pressure Drop

The overall analysis in Figure 10 demonstrates that augmenting the entrance velocity of the gas-solid stream leads to a corresponding enhancement in the efficiency of particle collection within the cyclone. An analysis of the predicted particle-collection efficiencies based on different turbulence models and experimental data revealed a consistent pattern [8], suggesting that there was no notable disparity among them. This holds for all turbulent flow models. Nevertheless, let us now direct our attention towards the meticulous comparison of the empirical data with the projected outcomes of particle-collecting efficiency. In this study, it is seen that the Reynolds Stress Model (RSM) has superior performance compared to the other four models (Spalart-Allmaras model,  $k-\epsilon$  standard, RNG  $k-\epsilon$ , and  $k-\omega$ ) in forecasting the cyclone collection efficiency. This superiority can be attributed to its strong correlation with the actual data. The Reynolds Stress Model turbulence provided precise predictions of the collection efficiency, with percentage error margins of 0.85%, 1.2%, 0.8%, 3.37%, and 1.9% for each subsequent change in inlet velocity. Moreover, the Reynolds Stress Model consistently achieved a percentage error of less than 4 % for all inlet velocity fluctuations, thus emphasizing its exceptional precision in forecasting collection efficiency.

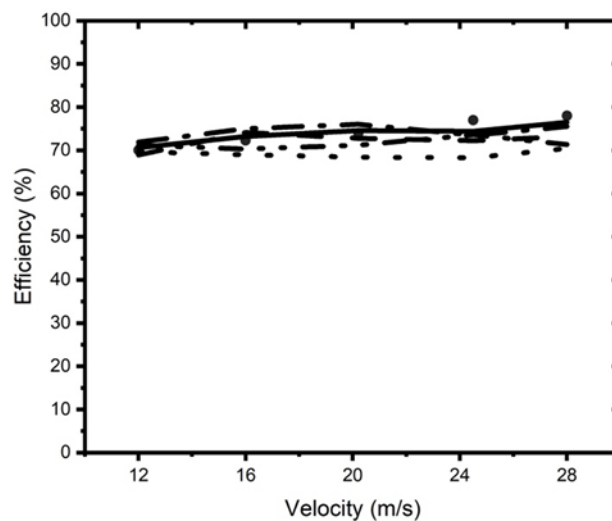


**Fig. 10.** Comparison between predictions of collection efficiency by various turbulence models with experimental data (symbol = experimental data; line = predicted results; — RSM; - - Spalart-Allmaras; ....  $k-\epsilon$  standard; - · - RNG  $k-\epsilon$ ; - · · -  $k-\omega$  standard)

Figure 11 presents a comparative analysis of the predicted pressure drop values at various inlet velocities utilizing several turbulence models, including RSM, Spalart-Allmaras,  $k-\epsilon$  standard, RNG  $k-\epsilon$ , and  $k-\omega$ . The simulation results indicate that an increase in the gas flow velocity entering the cyclone leads to a corresponding increase in the pressure drop, reflecting an increased energy requirement for cyclone operation. Similar to the predictions for collection efficiency, the qualitative differences in the predicted pressure drop values among the turbulence models were minimal.

However, when assessed quantitatively, the RSM demonstrated superior predictive accuracy compared to the Spalart-Allmaras,  $k-\epsilon$  standard, RNG  $k-\epsilon$ , and  $k-\omega$  models. RSM incorporates terms that account for the effects of streamlined curves, eddies, spins, and abrupt flow changes, resulting in more precise predictions of turbulent flows at high Reynolds numbers. Overall, the simulation results revealed an accumulated error of less than 10%, indicating that the RSM provides a highly accurate representation of the pressure drop value.

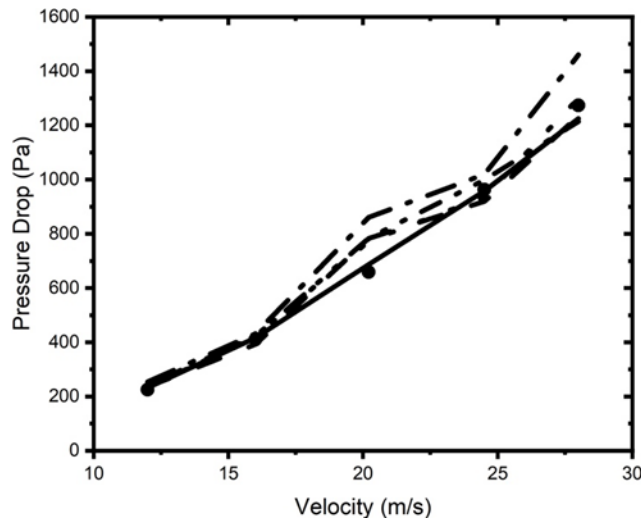


**Fig. 11.** Comparison between predicted pressure drop by various turbulence models and experimental data (symbol = experimental data; line = predicted result; – RSM; – – Spalart-Allmaras; .....  $k-\epsilon$  standard; - · - RNG  $k-\epsilon$ ; - · -  $k-\omega$  standard)

Figure 12 illustrates the predicted grade efficiency values at various diameter particles using several turbulence models, including RSM, Spalart-Allmaras,  $k-\epsilon$  standard, RNG  $k-\epsilon$ , and  $k-\omega$ . The simulation results indicate that as the diameter of the particles injected into the cyclone increases, the efficiency of the particle separation and collection also improves. Qualitatively, all the models exhibited the same trend, showing no significant differences in their predictions. However, quantitatively, the Reynolds Stress Model (RSM) demonstrated the best predictive accuracy, with a minor per cent error of 34%. In comparison, the per cent errors for the Spalart-Allmaras,  $k-\epsilon$  standard, RNG  $k-\epsilon$ , and  $k-\omega$  models are 34.17%, 48.43%, 38.69%, and 35.10%, respectively. This highlights the superior performance of the RSM in accurately predicting the separation efficiency in cyclone operations.

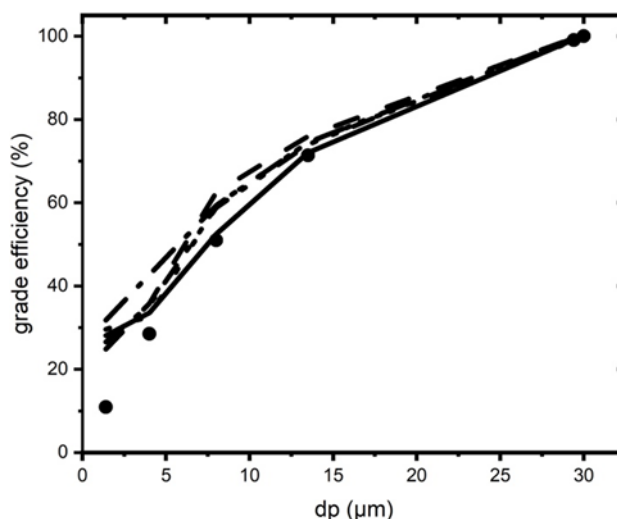


**Fig. 12.** Comparison between predicted grades of particle separation efficiency by various turbulence models with experimental data (symbol = experimental data; line = predicted result; – RSM; – – Spalart-Allmaras; ···· k- $\epsilon$  standard; - · - RNG k- $\epsilon$ ; - ··· - k- $\omega$  standard)

#### 4. Conclusions

The research targeted the performance of turbulence models in the prediction of efficiency and pressure drop of square cyclones. The results obtained from the simulation showed that the Reynolds Stress Model (RSM) was superior in predicting pressure drop and particle separation efficiency in cyclones compared with other models, including Spalart-Allmaras, standard k- $\epsilon$ , RNG k- $\epsilon$ , and k- $\omega$ . The agreement of RSM with the experimental data was pretty good and accurate predictions about the overall flow pattern were derived. However, RNG k- $\epsilon$  forecasts maximum tangential and axial velocity values. Therefore, for predictions intended to simulate cyclone performance and flow fields, the Reynolds Stress model is recommended. In case there are limitations regarding computational resources or time for using RSM, the RNG k- $\epsilon$  model becomes a viable alternative in predicting flow fields. The RSM or RNG k- $\epsilon$  selection should be made based on the specific needs of the simulation and weighed against the accuracy demands of the simulation with a trade-off with the computing expense.

This study can be viewed as not completely independent, as it is based on specific cyclone geometry and operational parameters. Future research may focus on geometric effects on cyclone efficacy, transcending various cyclone dimensions, investigations of sensitivity, and hybrid models that combine the advantages of RSM and RNG k- $\epsilon$  toward better performance prediction. This work deepened our understanding of the choice of turbulence model for cyclone separator simulations naming the Reynolds Stress model as the most credible.

#### Acknowledgement

The authors would like to express their gratitude to Syiah Kuala University for the financial support provided for this research through the Syiah Kuala University H-Index Research Program under contract no. 311/UN11.2.1/PT.01.03/PNBP/2021.

## References

- [1] Elehinafe, Francis B., Ephraim A. Aondoakaa, Akinnike F. Akinyemi, Oluranti Agboola, and Oyetunji B. Okedere. "Separation processes for the treatment of industrial flue gases-Effective methods for global industrial air pollution control." *Heliyon* (2024). <https://doi.org/10.1016/j.heliyon.2024.e32428>
- [2] Yohana, Eflita, Mohammad Tauviqirrahman, Arbian Ridzka Putra, Ade Eva Diana, and Kwang-Hwan Choi. "Numerical analysis on the effect of the vortex finder diameter and the length of vortex limiter on the flow field and particle collection in a new cyclone separator." *Cogent Engineering* 5, no. 1 (2018): 1562319. <https://doi.org/10.1080/23311916.2018.1562319>
- [3] Wang, Shurong, Mengxiang Fang, Zhongyang Luo, Xuantian Li, Mingjiang Ni, and Kefa Cen. "Instantaneous separation model of a square cyclone." *Powder Technology* 102, no. 1 (1999): 65-70. [https://doi.org/10.1016/S0032-5910\(98\)00196-X](https://doi.org/10.1016/S0032-5910(98)00196-X)
- [4] Junfu, Lu, Zhang Jiansheng, Zhang Hai, Liu Qing, and Yue Guangxi. "Performance evaluation of a 220t/h CFB boiler with water-cooled square cyclones." *Fuel Processing Technology* 88, no. 2 (2007): 129-135. <https://doi.org/10.1016/j.fuproc.2004.12.008>
- [5] Xiong, B., X. F. Lu, R. S. Amano, and C. Shu. "Experimental research on gas-solid flow in a square cyclone separator with double inlets." In *Proceedings of the 20th International Conference on Fluidized Bed Combustion*, pp. 393-397. Springer Berlin Heidelberg, 2010. [https://doi.org/10.1007/978-3-642-02682-9\\_58](https://doi.org/10.1007/978-3-642-02682-9_58)
- [6] Malahayati, Nur, D. Darmadi, Cut Alisa Putri, Lia Mairiza, Wahyu Rinaldi, and Y. Yunardi. "Comparative performance analysis between conventional and square cyclones for solid particle-gas separation: a review." *Materials Today: Proceedings* 63 (2022): S318-S325. <https://doi.org/10.1016/j.matpr.2022.03.157>
- [7] Fatahian, Hossein, Esmaeel Fatahian, Majid Eshagh Nimvari, and Goodarz Ahmadi. "Novel designs for square cyclone using rounded corner and double-inverted cones shapes." *Powder Technology* 380 (2021): 67-79. <https://doi.org/10.1016/j.powtec.2020.11.034>
- [8] Su, Yaxin, and Yuru Mao. "Experimental study on the gas-solid suspension flow in a square cyclone separator." *Chemical Engineering Journal* 121, no. 1 (2006): 51-58. <https://doi.org/10.1016/j.cej.2006.04.008>
- [9] Wasilewski, Marek, Lakhbir Singh Brar, and Grzegorz Ligus. "Experimental and numerical investigation on the performance of square cyclones with different vortex finder configurations." *Separation and Purification Technology* 239 (2020): 116588. <https://doi.org/10.1016/j.seppur.2020.116588>
- [10] Westerweel, Jerry, Gerrit E. Elsinga, and Ronald J. Adrian. "Particle image velocimetry for complex and turbulent flows." *Annual Review of Fluid Mechanics* 45, no. 1 (2013): 409-436. <https://doi.org/10.1146/annurev-fluid-120710-101204>
- [11] Raoufi, Arman, Mehrzad Shams, and Homayoon Kanani. "CFD analysis of flow field in square cyclones." *Powder Technology* 191, no. 3 (2009): 349-357. <https://doi.org/10.1016/j.powtec.2008.11.007>
- [12] Su, Yaxin, Anqiao Zheng, and Bingtao Zhao. "Numerical simulation of effect of inlet configuration on square cyclone separator performance." *Powder Technology* 210, no. 3 (2011): 293-303. <https://doi.org/10.1016/j.powtec.2011.03.034>
- [13] Safikhani, H., M. Shams, and S. Dashti. "Numerical simulation of square cyclones in small sizes." *Advanced Powder Technology* 22, no. 3 (2011): 359-365. <https://doi.org/10.1016/j.appt.2010.05.003>
- [14] Hosseini, Ebrahim. "Performance assessment of a square cyclone influenced by inlet section modifications." *Journal of the Brazilian Society of Mechanical Sciences and Engineering* 42, no. 10 (2020): 515. <https://doi.org/10.1007/s40430-020-02606-w>
- [15] Chaghakaboodi, Hooman Abdi, and Maysam Saidi. "Numerical study of gas-solid flow in a square cyclone separator with different vortex finders." *Chemical Engineering Research and Design* 194 (2023): 621-635. <https://doi.org/10.1016/j.cherd.2023.05.001>
- [16] Venkatesh, S., R. Suresh Kumar, S. P. Sivapirakasam, M. Sakthivel, D. Venkatesh, and S. Yasar Arafath. "Multi-objective optimization, experimental and CFD approach for performance analysis in square cyclone separator." *Powder Technology* 371 (2020): 115-129. <https://doi.org/10.1016/j.powtec.2020.05.080>
- [17] Meza, Hector Zambrano, and Linda Margarita Medina. "Application of Computational Fluid Dynamics to Study the Influence of Turbulence Models in the Behavior of the Cyclonic Separators." *International Journal of Petrochemical Science & Engineering* 2, no. 2 (2017): 66-72. <https://doi.org/10.15406/ipcse.2017.02.00033>
- [18] Fatahian, Hossein, Esmaeel Fatahian, and Rasool Erfani. "Square cyclone separator: performance analysis optimization and operating condition variations using CFD-DPM and Taguchi method." *Powder Technology* 428 (2023): 118789. <https://doi.org/10.1016/j.powtec.2023.118789>
- [19] Safikhani, Hamed, and Pegah Mehrabian. "Numerical study of flow field in new cyclone separators." *Advanced Powder Technology* 27, no. 2 (2016): 379-387. <https://doi.org/10.1016/j.appt.2016.01.011>

- [20] Mazyan, W. I., A. Ahmadi, J. Brinkerhoff, H. Ahmed, and M. Hoorfar. "Enhancement of cyclone solid particle separation performance based on geometrical modification: Numerical analysis." *Separation and Purification Technology* 191 (2018): 276-285. <https://doi.org/10.1016/j.seppur.2017.09.040>
- [21] Fatahian, Esmaeel, and Hossein Fatahian. "Computational fluid dynamics modeling of effect of dipleg geometry on separation efficiency of a square cyclone." *AUT Journal of Mechanical Engineering* 5, no. 3 (2021): 451-464.
- [22] Wei, Qing, Guogang Sun, and Cuizhi Gao. "Numerical analysis of axial gas flow in cyclone separators with different vortex finder diameters and inlet dimensions." *Powder Technology* 369 (2020): 321-333. <https://doi.org/10.1016/j.powtec.2020.05.038>
- [23] Safikhani, H., M. A. Akhavan-Behabadi, M. Shams, and M. H. Rahimyan. "Numerical simulation of flow field in three types of standard cyclone separators." *Advanced Powder Technology* 21, no. 4 (2010): 435-442. <https://doi.org/10.1016/j.appt.2010.01.002>
- [24] Surahmanto, Fredy, Aji Pamungkas, Dhimas Agung Mutoha, Arianto Leman Soemawidagdo, Beni Tri Sasongko, Sukardi Sukardi, Raihan Lutfianto, and Muhammad Rizky Pratama Hakim. "Performance Evaluation of Square Cyclone Separator with Cone Geometry Variations." *CFD Letters* 16, no. 7 (2024): 136-149. <https://doi.org/10.37934/cfdl.16.7.136149>
- [25] Hoekstra, A. J., J. J. Derksen, and H. E. A. Van Den Akker. "An experimental and numerical study of turbulent swirling flow in gas cyclones." *Chemical Engineering Science* 54, no. 13-14 (1999): 2055-2065. [https://doi.org/10.1016/S0009-2509\(98\)00373-X](https://doi.org/10.1016/S0009-2509(98)00373-X)